Supporting Information For

# Carrier Control of $MoS_2$ Nanoflakes by Functional Self-Assembled Monolayers

*Yang Li[†], Cheng-Yan Xu[†,‡]*, PingAn Hu[‡] and Liang Zhen[†,‡]**

[†]School of Materials Science and Engineering, Harbin Institute of Technology, Harbin 150001, China, [‡]MOE Key Laboratory of Micro-systems and Micro-structures Manufacturing, Harbin Institute of Technology, Harbin 150080, China

E-mail: lzhen@hit.edu.cn; cy_xu@hit.edu.cn;

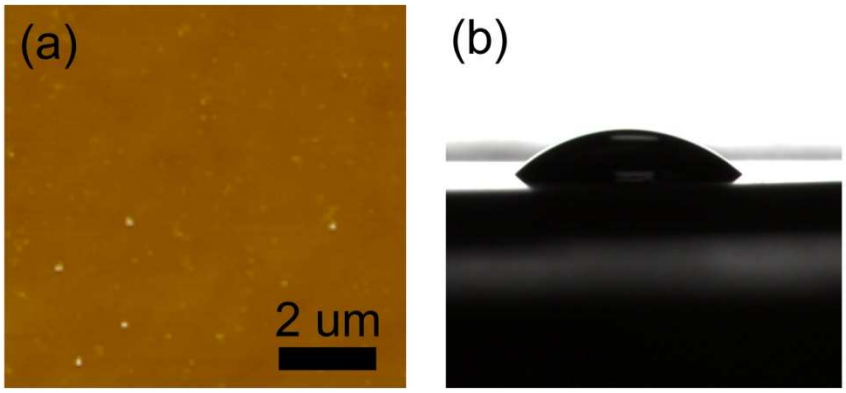


**Figure S1.** (a) AFM topography of Si substrate with a 300 nm thick oxide layer. The roughness of $SiO_2$ substrate is 0.46 nm. (b) The water contact angle of the pristine Si substrate treated by piranha solution.

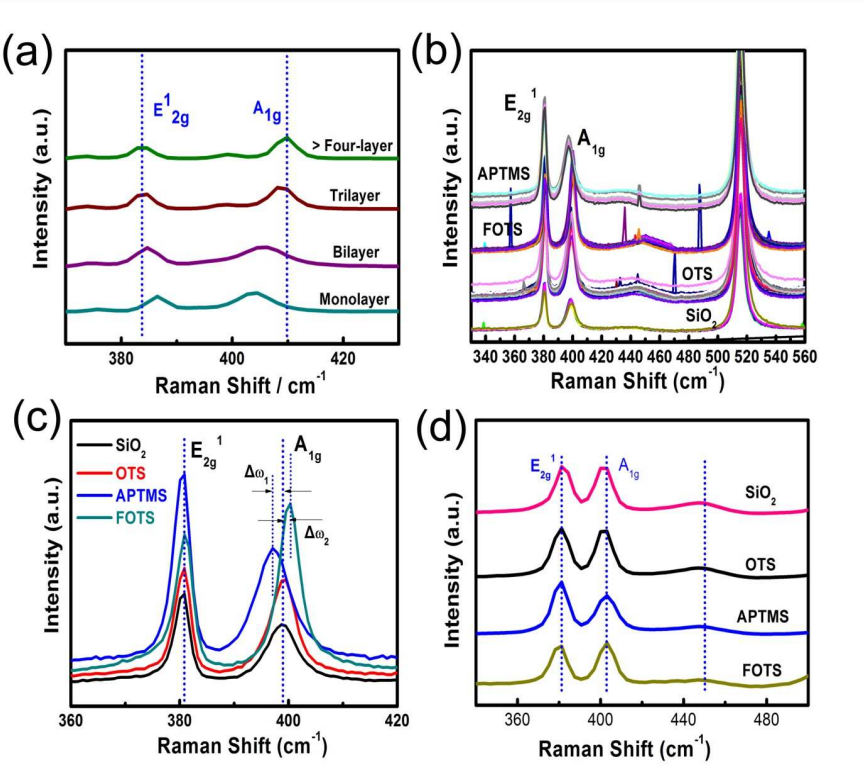


**Figure S2.** (a) Raman spectra of $MoS_2$ nanoflakes on pristine $SiO_2$ substrates. (b) Raman spectra of monolayer $MoS_2$ on the pristine and SAMs-modified substrates. The Raman mode of Si is not dependent on SAMs molecules. Therefore, the relative Raman shifts of $E_{2g}^1$ and $A_{1g}$ mode are calculated using Raman mode of Si as a reference. (c) The typical Raman spectra of monolayer $MoS_2$ on the pristine and SAMs-modified substrates according to Figure S2a. (d) The typical Raman spectra of pristine and SAMs-modified bilayer $MoS_2$ nanoflakes.

Figure S2a presents the Raman spectra of pristine $MoS_2$ nanoflakes. For monolayer $MoS_2$, there are two prominent Raman modes: out-of-plane mode $E_{2g}^1$ and in-plane mode $A_{1g}$, and the peaks distance is about 18.7 $cm^{-1}$. $E_{2g}^1$ presents redshift with increasing thicknesses of $MoS_2$ nanoflakes, while $A_{1g}$ shows blueshift. From Figure S2d, the positions and shapes of $E_{2g}^1$ and $A_{1g}$ modes are almost independent on SAMs molecules. The relative strong interlayer screening

effect and the weaker doping for bilayer $MoS_2$ lead to the unnoticeable variation of Raman modes by Raman spectroscopy.

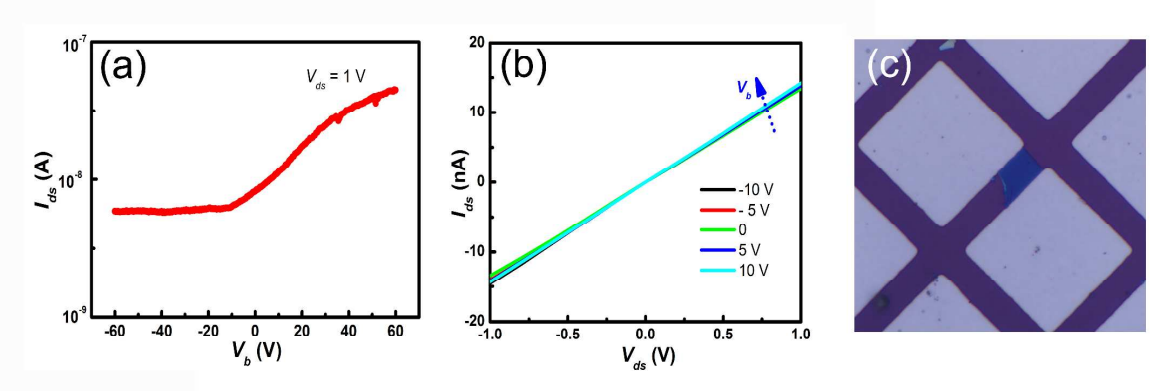


**Figure S3.** The transfer (a) and (b) output characteristics of FOTS- modified tri-layer $MoS_2$ device. The ON-state current and ON/OFF ratio are lowest, and the source-drain current ($I_{ds}$) does not vary significantly when the different gate voltage ($V_b$) is applied. (c) The typical configuration of the devices in our work. The channel length is 6 μm. The tilayer $MoS_2$ presents purple, and the size is relative large for the device fabrication.

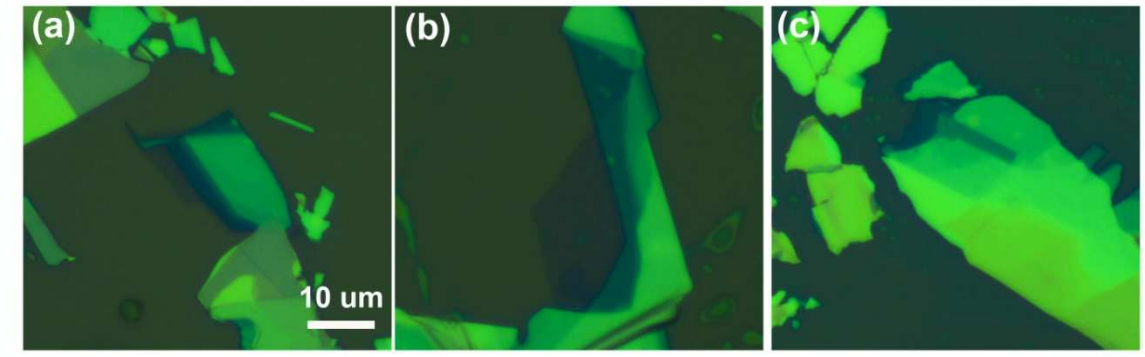


**Figure S4.** Optical images of $MoS_2$ nanoflakes on (a) pristine, (b) OTS-modifed, (c) FOTS-modified substrates, respectively.

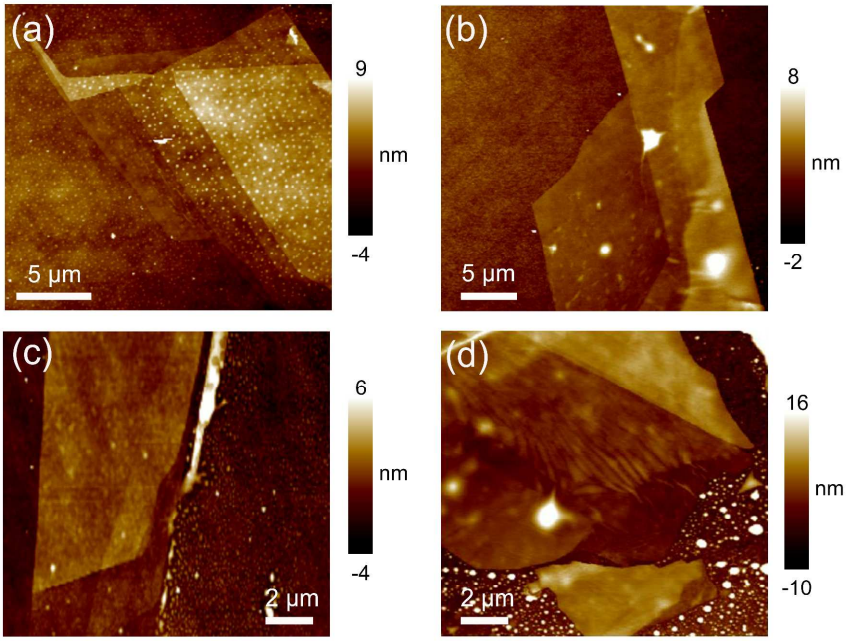


**Figure S5.** AFM images of $MoS_2$ nanoflakes on (a) pristine, (b) OTS-modifed, (c) APTMS-modified, and (d) FOTS-modified substrates, respectively.

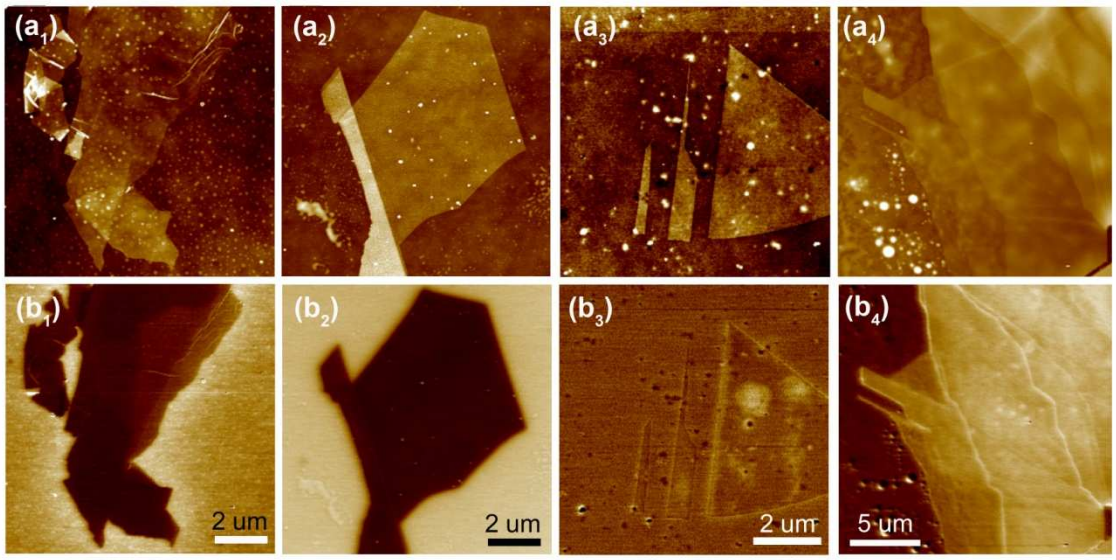


**Figure S6.** AFM topographies and surface potential maps of $MoS_2$ nanoflakes on the pristine and SAMs-modified $SiO_2$ substrates. ($a_1$-$d_1$) The topographies of $MoS_2$ nanoflakes on $SiO_2$, OTS, APTMS and FOTS. ($a_2$-$d_2$) The corresponding surface potential maps of $MoS_2$ nanoflakes shown in $a_1$-$d_1$.

In Figure S6, the surface potential of $MoS_2$ nanoflakes on pristine substrate decreases with the number of layer (shown in $a_1$ and $b_1$); the contact potential difference between tri-layer $MoS_2$ and 6-layer $MoS_2$ nanoflakes (shown in $a_2$ and $b_2$) presents no significant change; bilayer $MoS_2$ on ATPMS-modified substrate have the similar surface potential to APTMS-SAM (shown in $a_3$ and $b_3$). The surface potential of $MoS_2$ nanoflakes on FOTS-modified substrates increases with the number of layer (shown in $a_4$ and $b_4$).

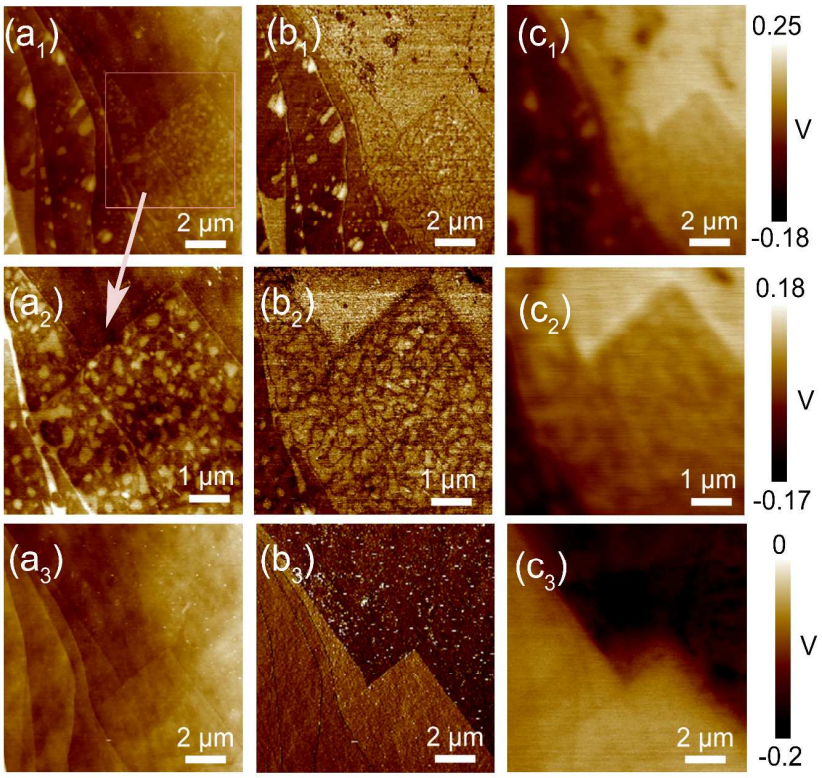


**Figure S7.** The topographies, phases and surface potential maps of the pristine and annealed $MoS_2$ nanoflakes on the pristine $SiO_2$ substrates.

The structure of $MoS_2$ can not be destroyed since the annealing temperature (230 ºC) is much lower than the phase transition temperature. As we have verified below (lines 101-107, Page S9), the sharp phase contrast in Figure S7$b_1$ indicates the formed water layers upon the pristine $MoS_2$ nanoflakes, while the trivial phase contrast in Figure S7$b_2$ (the enlarged area in Figure S7$a_1$) indicates the formed water layers underneath $MoS_2$ nanoflakes. Before annealing, the obvious surface potential difference can be observed, and the surface potential decreases by increasing the thicknesss. After annealing, the water layers upon or underneath $MoS_2$ nanoflakes are eliminated (as shown in Figure S7$b_3$, phase image), and the surface potential of annealed $MoS_2$ nanflakes is lower than that of the pristine samples (For monolayer $MoS_2$, the surface

potential decreases by 0.12±0.03 V after annealing). Meanwhile, it should be noting that the interlayer screening effect seems to be not obvious after annealing, as shown in Figure S7c$_3$.

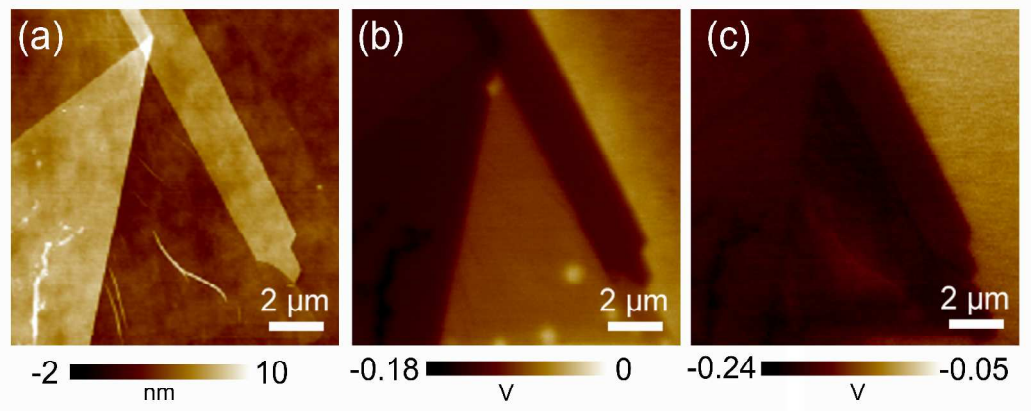


**Figure S8.** The topographies, phase and surface potential maps of the pristine and annealed $MoS_2$ nanoflakes on OTS-modified $SiO_2$ substrates.

OTS has strong hydrophobicity, and the water layer upon or underneath $MoS_2$ nanoflakes is not observed. $MoS_2$ nanoflakes modified by OTS are annealed at 140 ºC for 4 h. The lower annealing temperature is applied to avoid the destruction of OTS. Compared with the pristine samples (shown in Figure S8b), the surface potential of annealed $MoS_2$ shown in Figure S8c also lowers (For monolayer $MoS_2$, the surface potential decreases by 0.10±0.02 V after annealing) and the weak interlayer screening effect of annealed $MoS_2$ nanoflakes is also observed.

From Figures S7, S8 and the corresponding explanations, we demonstrate the effects of the water molecules on the surface potential of $MoS_2$ nanoflakes. Before annealing, the distinct interlayer screening effect is observed, while after annealing the interlayer screening effect seems to be weak. For monolayer $MoS_2$, the surface potential decreases by about 0.10-0.12 V. The results demonstrate that the water molecules indeed shield the actual surface potential of $MoS_2$ nanoflakes, and the effect of water molecules is complicated, and need to be analyzed in depth.

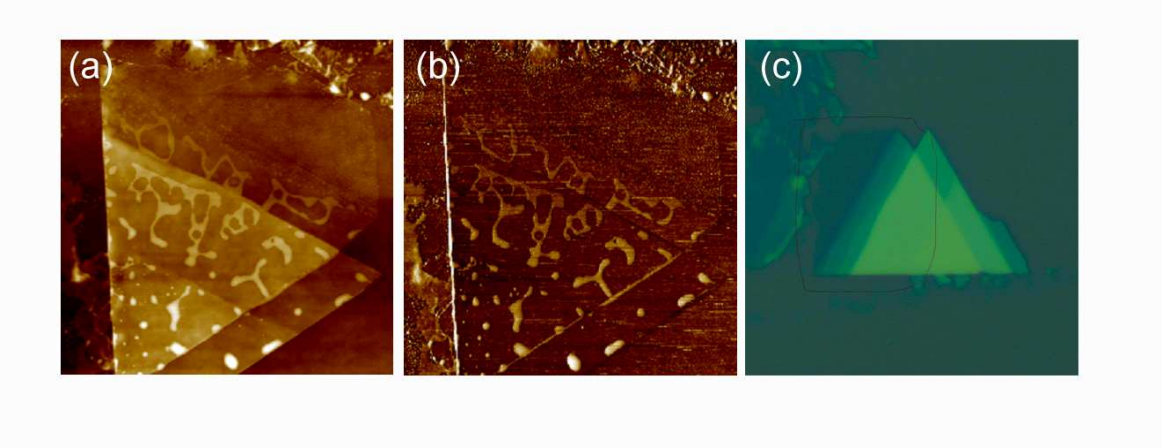


**Figure S9.** AFM topography (a) and the corresponding phase image (b) $MoS_2$ nanoflakes on the pristine $SiO_2$ substrate. (c) Optical images of $MoS_2$ nanoflakes on pristine $SiO_2$ substrates.

From the phase image (Figure S9b), the significant phase difference is observed between water layers and $MoS_2$ nanoflakes, reflecting the difference in surface potential. According to the relevant research about graphene, if the water layers exist underneath graphene, the phase difference will be trivial.[1,2] However, the large phase difference indicates that the AFM tip is interacting with the different surface ($MoS_2$ and water layers in our experiments), and the water layers absorb upon the $MoS_2$ nanoflakes. According to the AFM topography (Figure S9a), the height of the water layers is about 3 nm.

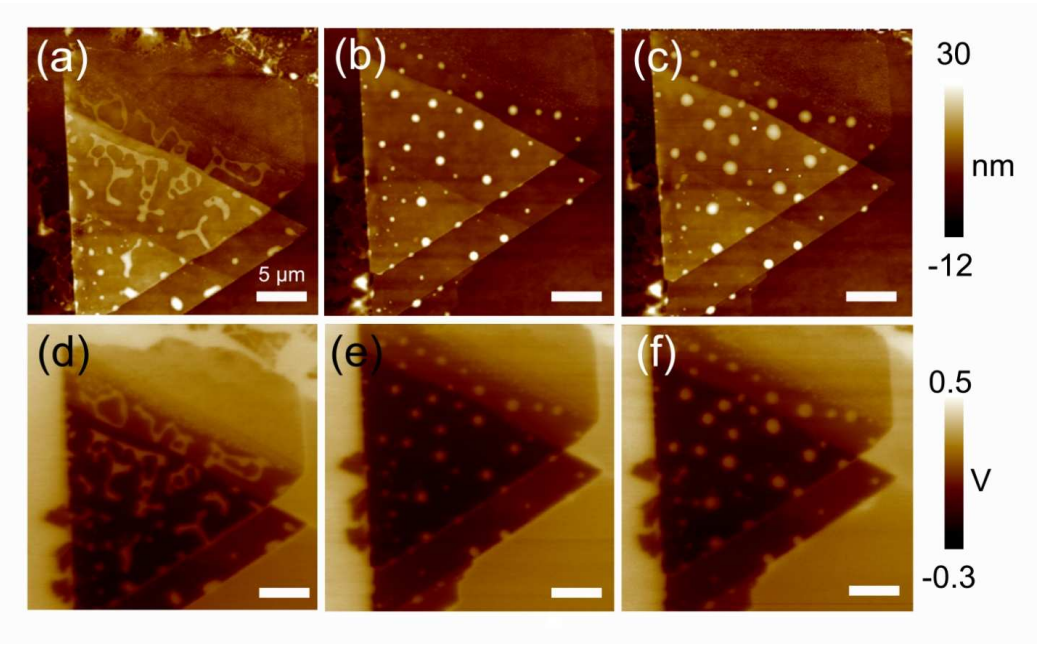


**Figure S10.** The topographies and the corresponding surface potential maps of $MoS_2$ nanoflakes on the pristine $SiO_2$ substrates. (a), (d) at room atmosphere 45%; (b), (e) 61%; (c), (f) 80 %.

By increasing the humidity, the height of the formed water layers increases from 3 nm to 21 nm. From Figure S10d-f, the surface potential of $MoS_2$ with water layers is lower than that of $MoS_2$ without water layers, verifying that the formed water layers shield the actual surface potential of $MoS_2$ nanoflakes.[3,4] It should be noted that the other areas of $MoS_2$ nanoflakes, which are not covered with the formed water layers, still absorbs external water molecules. However, the surface potential of $MoS_2$ nanoflakes without water layers keeps nearly constant when the humidity increases from 45% to 80%.

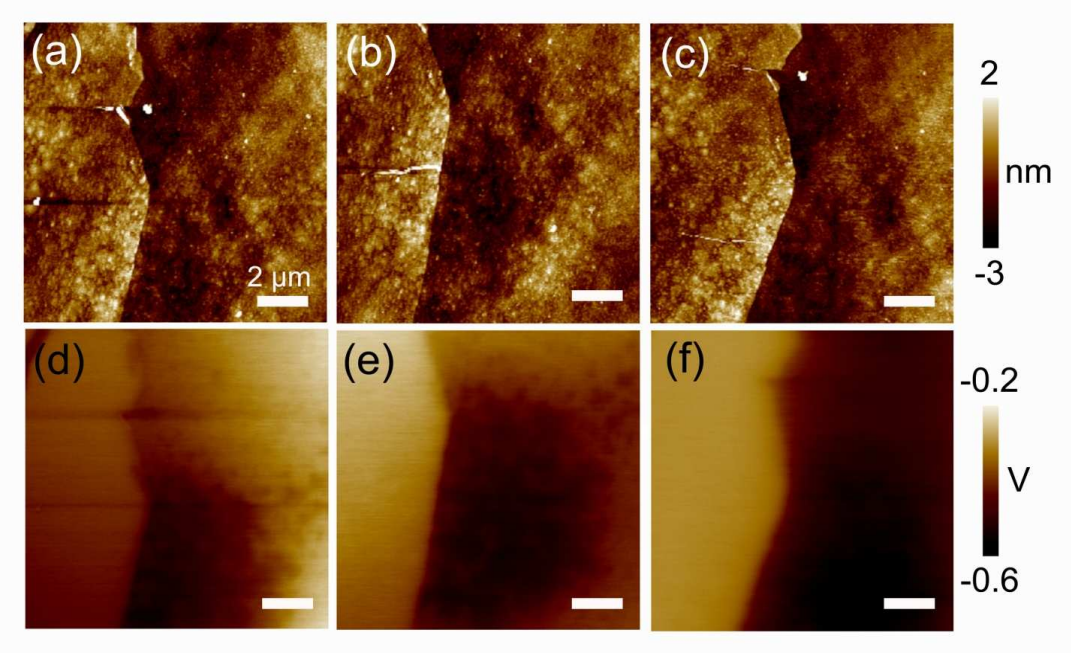


**Figure S11.** AFM topographies and the corresponding surface potential maps of $MoS_2$ nanoflakes on FOTS-modified monolayer $MoS_2$ at different relative humidity.(a), (d) at room atmosphere 45%; (b), (e) 65%; (c), (f) 78 %. The scale bars are all 2 μm.

The annealing experiments have demonstrated that the absorbed water moleules indeed have significant effects on the carrier distribution of $MoS_2$ nanoflakes. According to Figure S11, when the humidity increased from 45% to 78%, the surface potential of monolayer $MoS_2$ had little variation, indicating that the effect of the externally absorbed water molecules on the carrier distribution of $MoS_2$ is almost constant.

According to humidity and annealing experiments, KFM seems to be not the most reliable method to evaluate the interfacial charge transfer due to the significant effect of external atmosphere. The absorbed water molecules indeed shield the actual surface potential of $MoS_2$. Compared to the pristine $MoS_2$, the interlayer screening effect of annealed $MoS_2$ seems to become weaker. For monolayer $MoS_2$, the surface potential decreases by about 0.08-0.12 V.

Therefore, by eliminating the contribution of the absorbed water layers or molecules, we think that the actual Fermi level shift of monolayer $MoS_2$ is about 0.45-0.47 eV.

**REFERENCES**


S1. Xu, K.; Cao, P.; Heath, J. R., Graphene Visualizes the First Water Adlayers on Mica at Ambient Conditions. *Science* **2010,** *329*, 1188-1191.

S2. Shim, J.; Lui, C. H.; Ko, T. Y.; Yu, Y.-J.; Kim, P.; Heinz, T. F.; Ryu, S., Water-Gated Charge Doping of Graphene Induced by Mica Substrates. *Nano Lett.* **2012,** *12*, 648-654.

S3. Araujo, W.; Salvadori, M.; Teixeira, F.; Cattani, M.; Brown, I., Environmental Effects in Kelvin Force Microscopy of Modified Diamond Surfaces. *Microsc. Res. Tech.* **2012,** *75*, 977-981.

S4. Sugimura, H.; Ishida, Y.; Hayashi, K.; Takai, O.; Nakagiri, N., Potential Shielding by the Surface Water Layer in Kelvin Probe Force Microscopy. *Appl. Phys. Lett.* **2002,** *80*, 1459-1461.